Supplementary Material for Fabrication, Characterization, and Repair of NanoCarbon-Loaded Aircraft Paint-Based Sensors for Real-World SHM: Studies at the Laboratory Scale

by
Carlos Cuellar, Kaitlyn Watson, Elisabeth Smela

6 xGnP Preparation

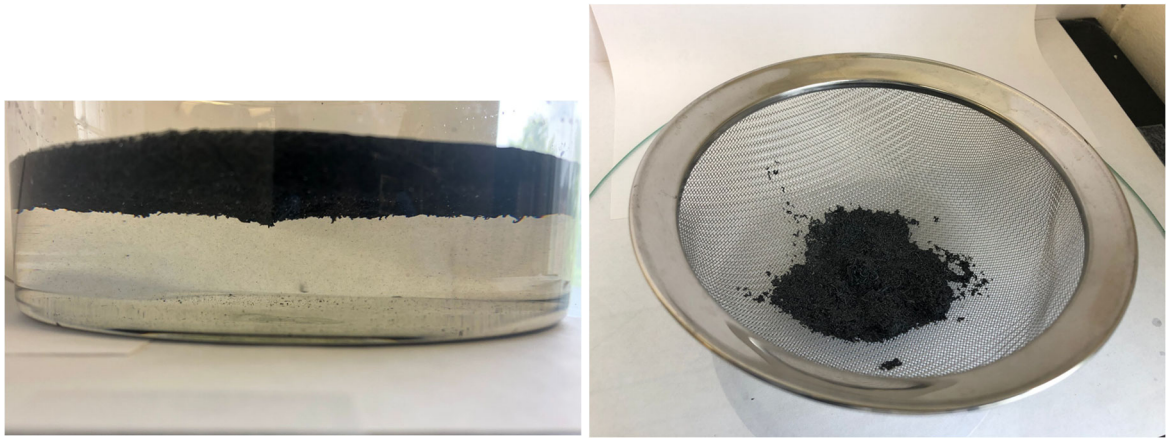


Figure 11. (left) Filtration of unexpanded graphite in water. xGnP floats and unexpanded graphite sinks. (right) Floating xGnP layer sieved to remove water.

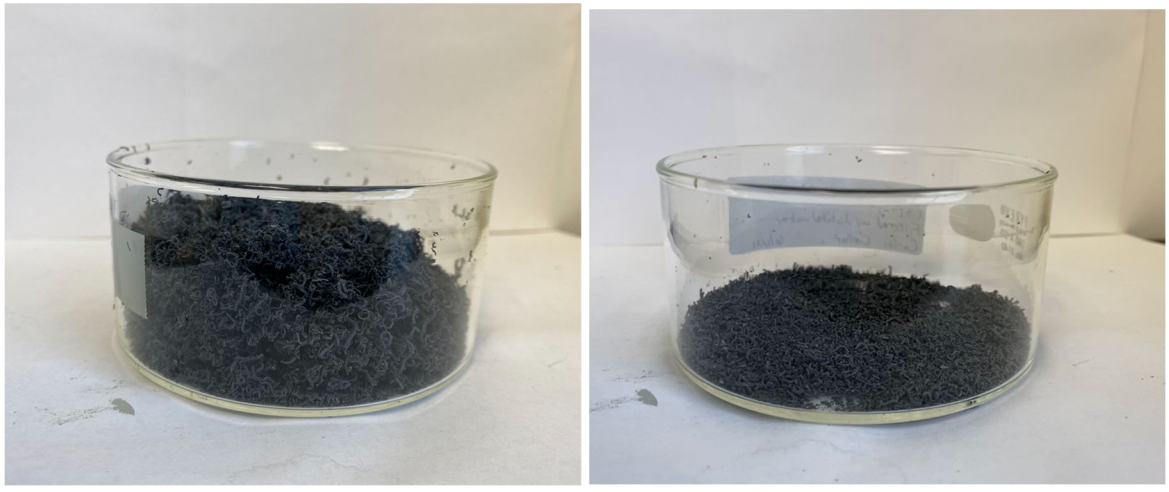


Figure 12. (left) xGnP before filtration. (right) xGnP after filtration and oven drying – the volume is reduced.

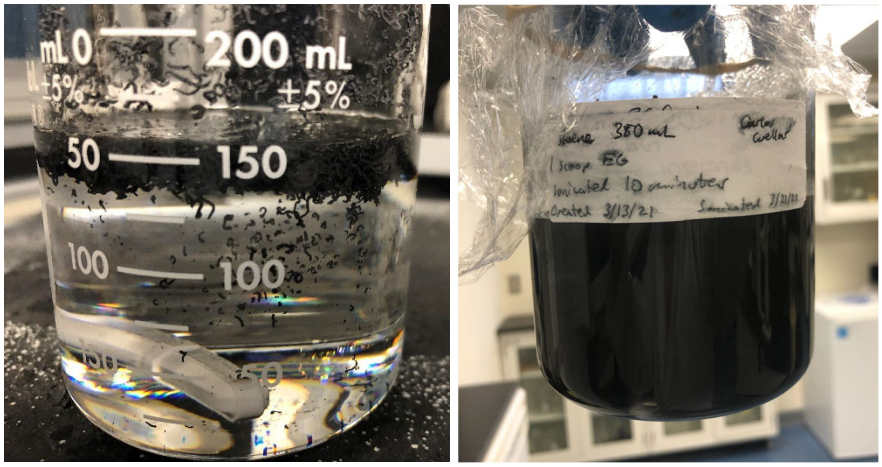
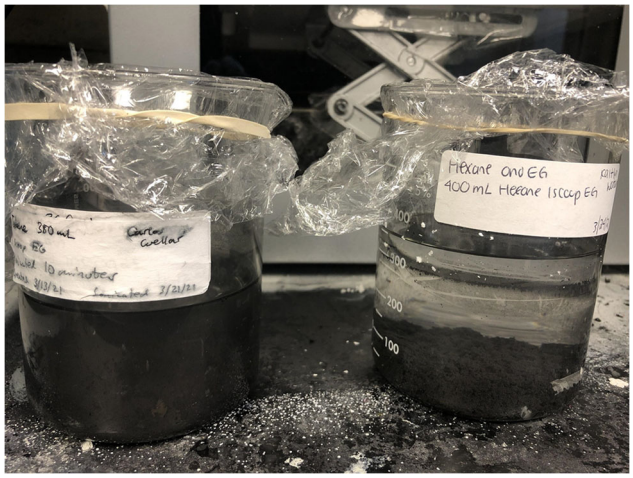


Figure 13. (left) xGnP in solvent prior to sonication. (right) xGnP in toluene just after sonication to 100 kJ.

a)



b)

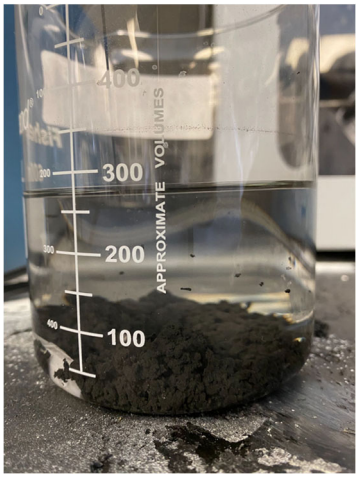


Figure 14. a) xGnP several days after sonication in toluene (left) and hexane (right). Some xGnP remained suspended in toluene, but there was xGnP settled on the bottom. In hexane there was no suspension. b) xGnP in ethyl acetate 2 days after sonication.

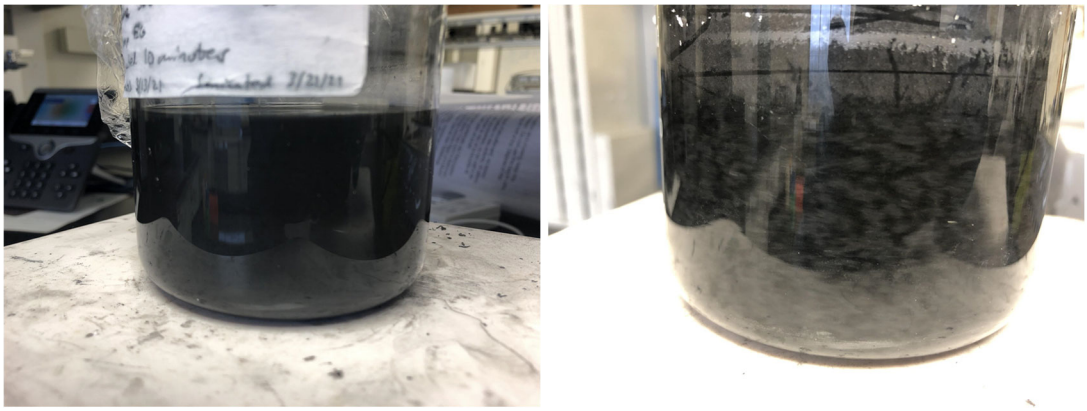


Figure 15. (left) After magnetic stirring, the xGnP in toluene re-suspended completely. (right) After magnetic stirring, the xGnP in hexane remained in clumps.

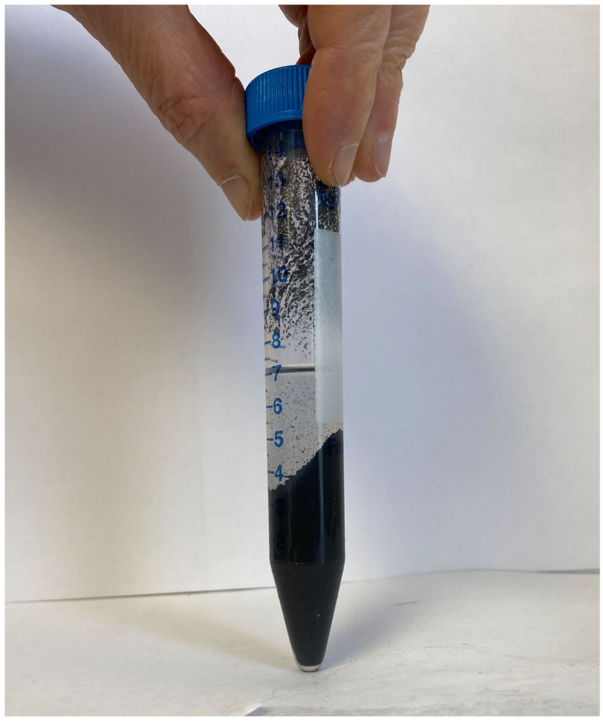
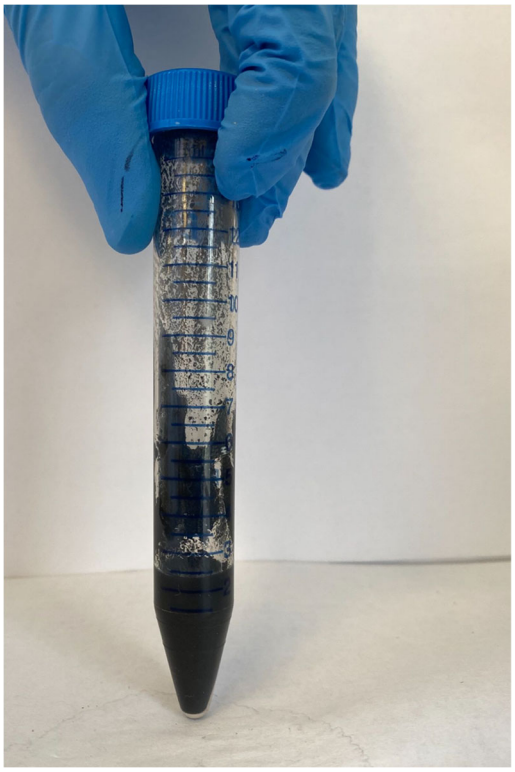
a)  b) 

Figure 16. a) xGnP in EA (7 mL total volume) and b) after removal of EA (2.5 mL total).

7 Microcontroller Circuit

The circuit is shown in Figure 17. One leg of the bridge had the sensor and a voltage-controlled resistor (Analog Devices digital pot, AD5206), the other had fixed resistors. The Arduino's analog read pins utilize 10-bit built-in analog to digital converters that read 0 to 5 V with a resolution of 4.89 mV. The voltage was maintained near 2 V by adjusting R_{pot1} to keep the op amp operating at the center of its range, where it is linear, to ensure accuracy. R_{pot2} and $R_{pot\ 3}$ controlled the gain of the op amp.

- The op amp is an Analog Devices OP27.
- R_{sg} is the sensor (strain gauge).
- R_{pot1} – R_{pot3} are voltage-controlled resistors.
- R_1- R_6 are fixed resistors.
- V_{in} comes from the Arduino's V_{out} pin.
- V_{out} goes to an Arduino analog in pin.

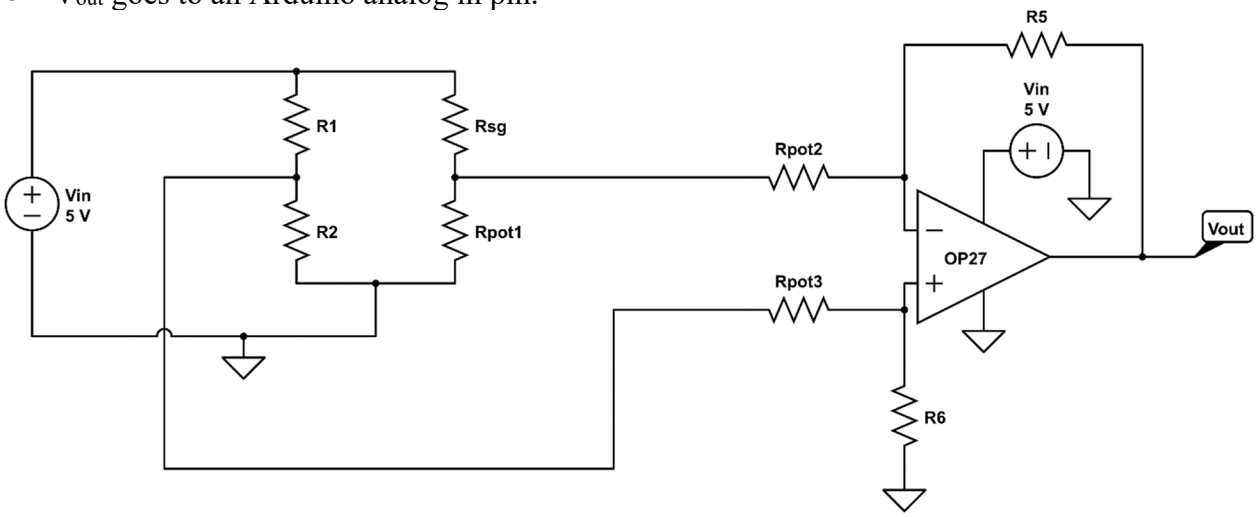


Figure 17. Circuit used to continuously record resistance data from the sensors.

8 Acrylic Spool Used for Constant Strain Measurements

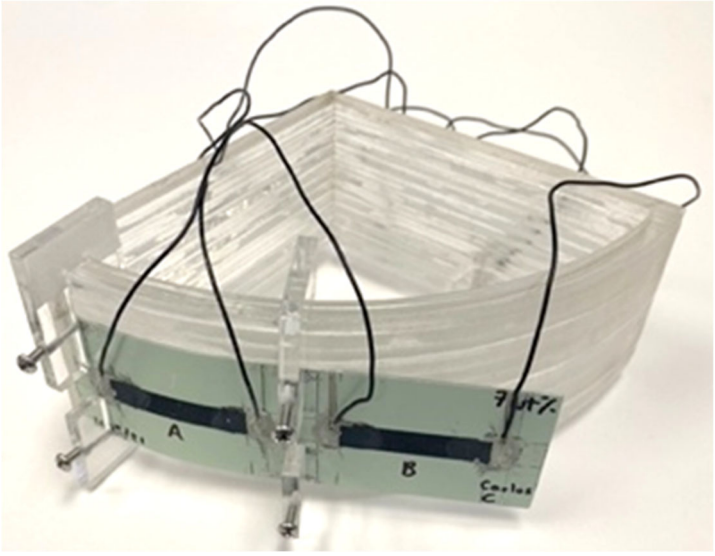


Figure 18. Acrylic spool of know radius to which the coupons were affixed using clips, here shown clamped to the outer surface for tensile strain face outward. The clips could be moved to strain just one gauge at a time, here gauge A, while leaving the other unstrained.

9 SEMs of xGnP

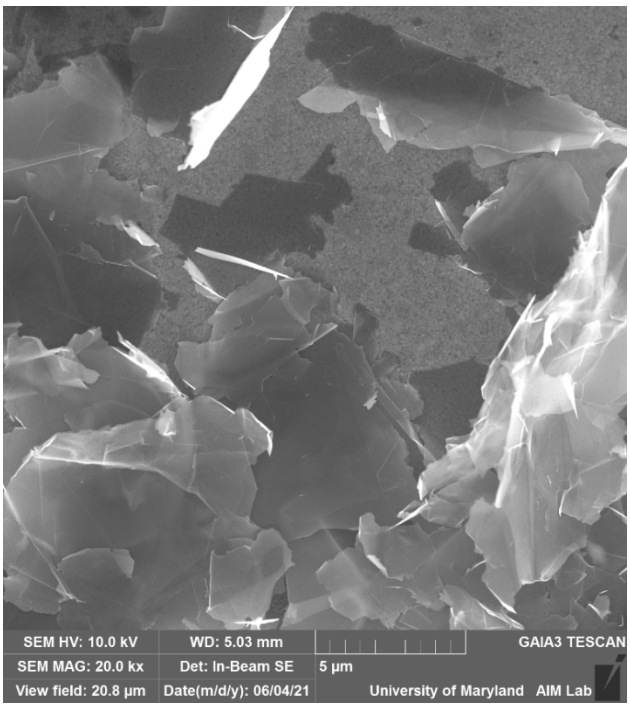
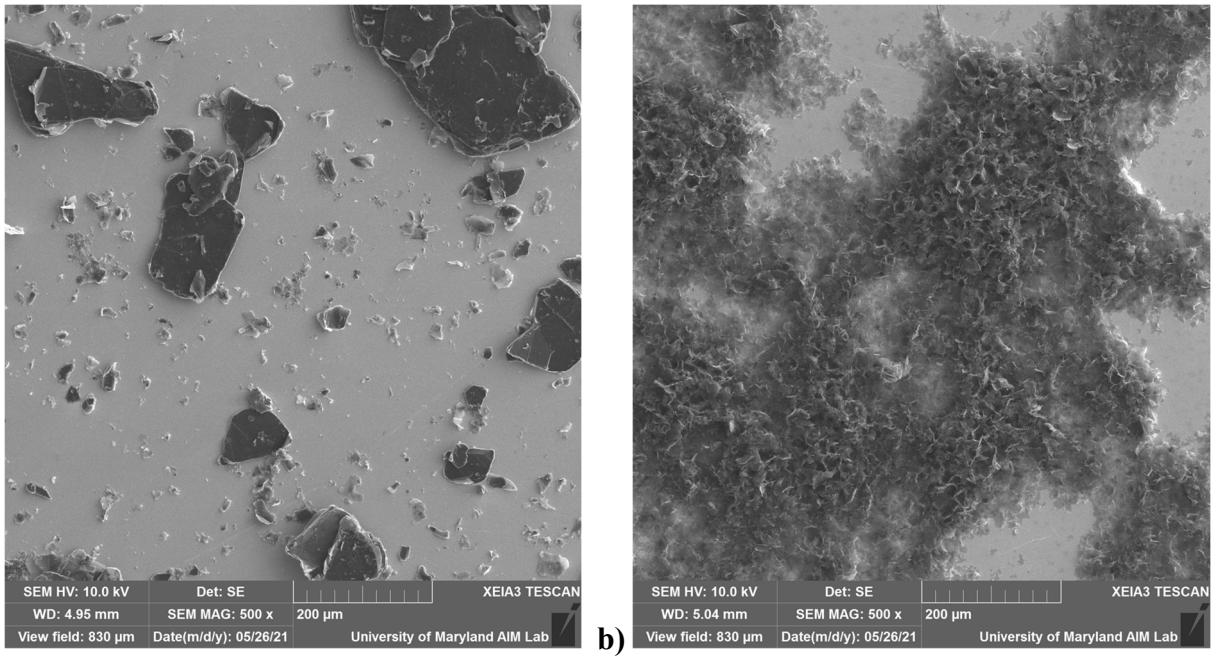


Figure 19. Scanning electron microscopy image of xGnP taken at 10 kV. (Tescan GAIA3)



a) **b)**

Figure 20. SEM images of a) unexpanded graphite flake post sonication and b) xGnP after sonication to 100 kJ.

10 Calculation of xGnP Loading

Table 2. Calculation of EA:topcoat ratios and xGnP wt% in film.

xGnP (g)	Ethyl Acetate (g)	AF3500 Topcoat (g)	EA:Imron AF3500 ratio	13110S Activator (g)	Total wet paint (g)	Total dry paint (g)	xGnP:dry paint ratio
0.28	9.04	3.68	2.46	1.89	5.57	3.78	6.9
0.28	5.75	2.66	2.16	1.31	3.97	2.70	9.5
0.28	6.05	1.65	3.67	0.84	2.49	1.69	14.3
0.28	7.74	0.84	9.21	0.44	1.28	0.87	24.5

11 Electrical Connections Over Flange

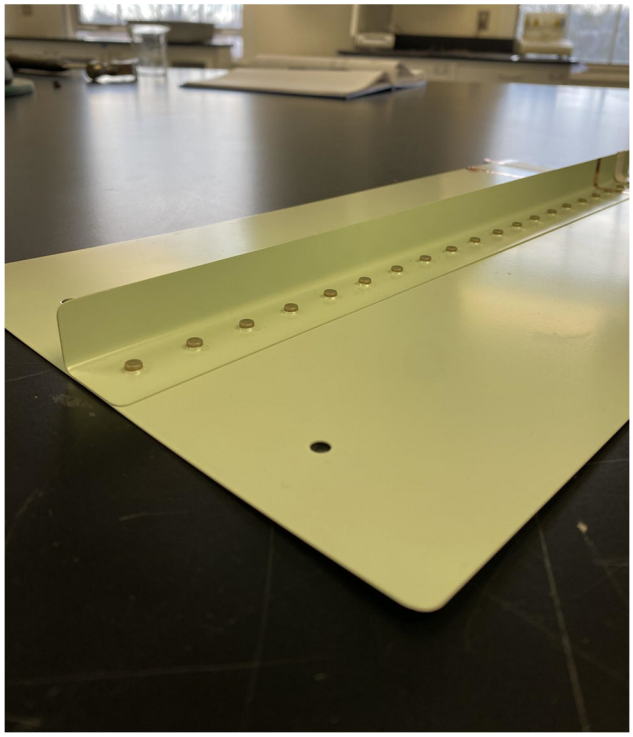


Figure 21. Example of aircraft skin (primed Al) with perpendicular flange and exposed metal rivets.

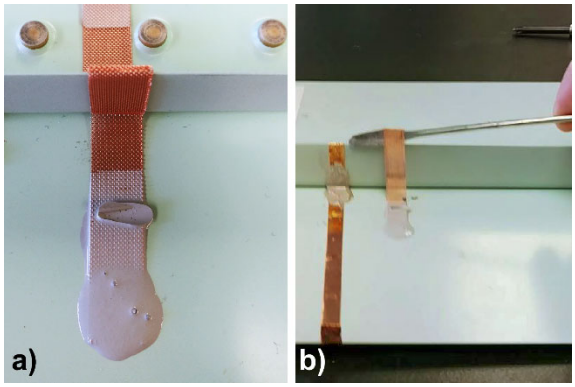


Figure 22. a) Concept of using Cu mesh to jump over a flange on a surface. The mesh is attached to the surface using Imron paint (in this case without xGnP). b) Al part with flange suspended by lifting the Cu mesh connection. (On the left is a strip of Cu tape.)

12 Contact Resistance to Cu Paint

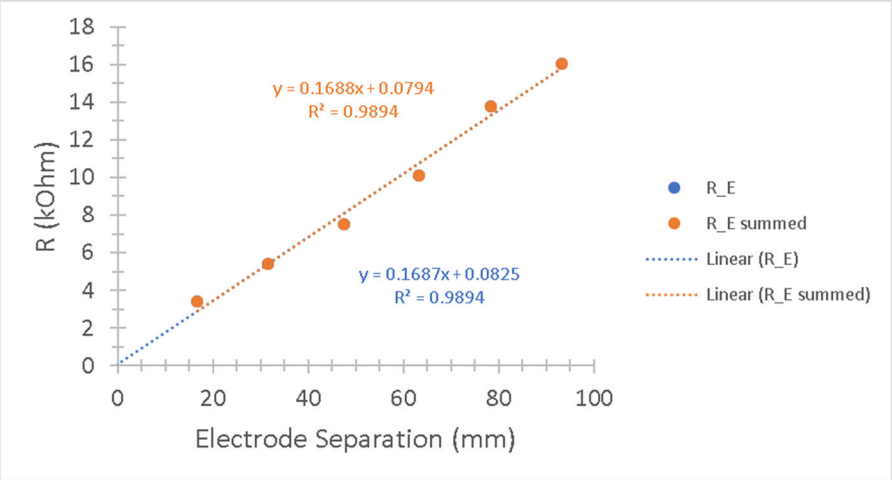


Figure 23. Resistance between Cu paint electrodes separated by the given length (blue) and resistance obtained by summing the resistances between adjacent electrodes to reach the total length (orange). Linear fits are shown.

The contact resistance between the xGnP paint and the electrodes was shown to be negligible compared to the xGnP paint resistance by two measures. First, the intercept of a resistance versus electrode separation plot was on the order of 80 Ω. Given the scatter in the data, due to film thickness variations, there is some uncertainty in this value. Second, and perhaps more tellingly, the resistance between electrodes separated by a certain distance was the same as the resistance obtained by summing the resistances between sets of adjacent electrodes to that length. If the contact resistance had been large, the latter value would have been higher, due to the cumulative addition of the contact resistances at each stage. At a separation of 93 mm, the difference in these values was less than 10 Ω.

13 Sensor Preparation Photographs

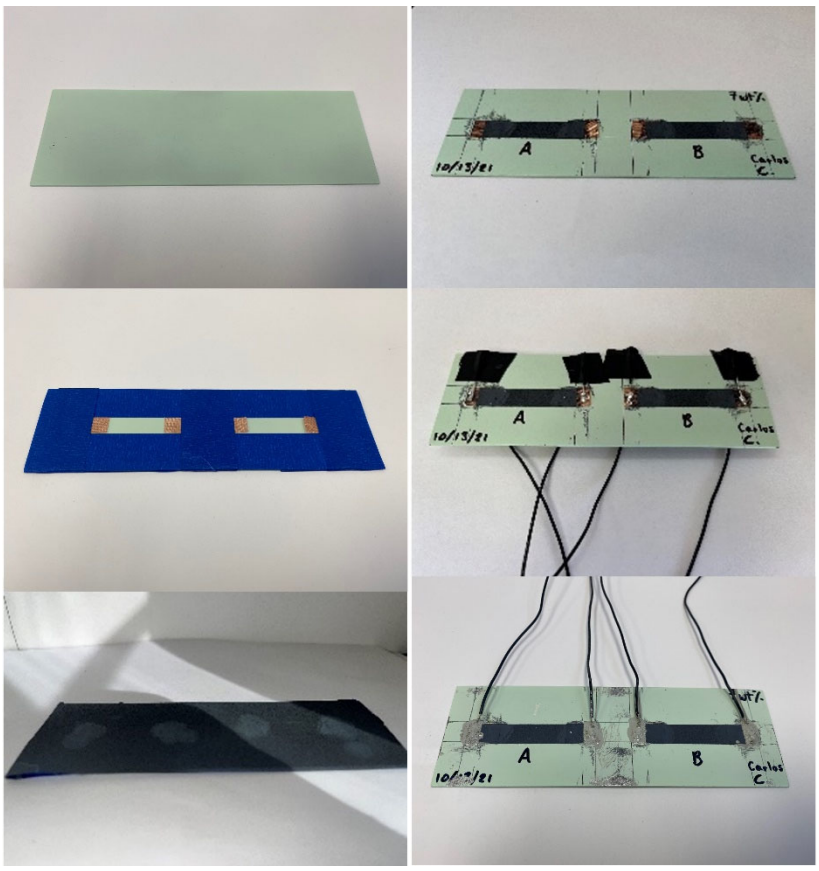


Figure 24. Photographs corresponding to the illustrations in Figure 1.

14 Sensor Thickness by Profilometry

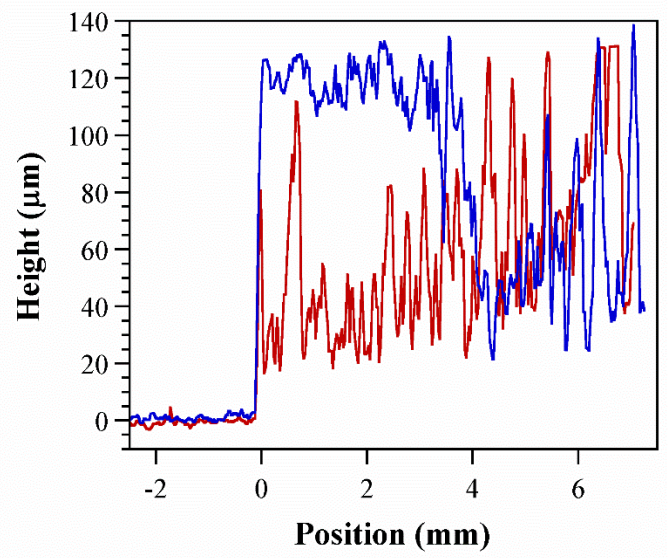


Figure 25. Height as a function of position across the sensor width, taken at two places along its length, for a 7 wt% xGnP sensor formed by spray-coating. Points before position 0 were on the primed Al substrate.

The thickness of the sensors was measured by mechanical profilometry (Dektak ST 3030). The sensors were non-uniform in thickness, due to the hand-made fabrication, as shown by the profilometer scans in Figure 25. Thicknesses for spray-coated sensors (3 coats) ranged from 20-120 µm. Brush-coated sensors were thicker.

15 Percolation Threshold

As mentioned in the main text, given the non-uniformity of film thickness, it proved impossible to obtain consistent film resistivities. Therefore, a thickness of 60 μm was assumed for all the films to obtain an approximate value. The data in Figure 2b were fit with a standard power law relationship to find the percolation threshold:

(4) $$\sigma = \sigma_0 \left(\phi - \phi_c\right)^t,$$

where ϕ is the filler fraction, ϕ_c is the percolation threshold, and the exponent t characterizes the abruptness of the transition [22,80,93] (Figure 26a). Using $\sigma_0 = 24.8$, $\phi_c = 6.10\%$, and $t = 0.86$, the data and the model correlate with $R^2 = 0.996$ (Figure 26b). (Small values of t were discussed in polymer-CNT composites in [94].)

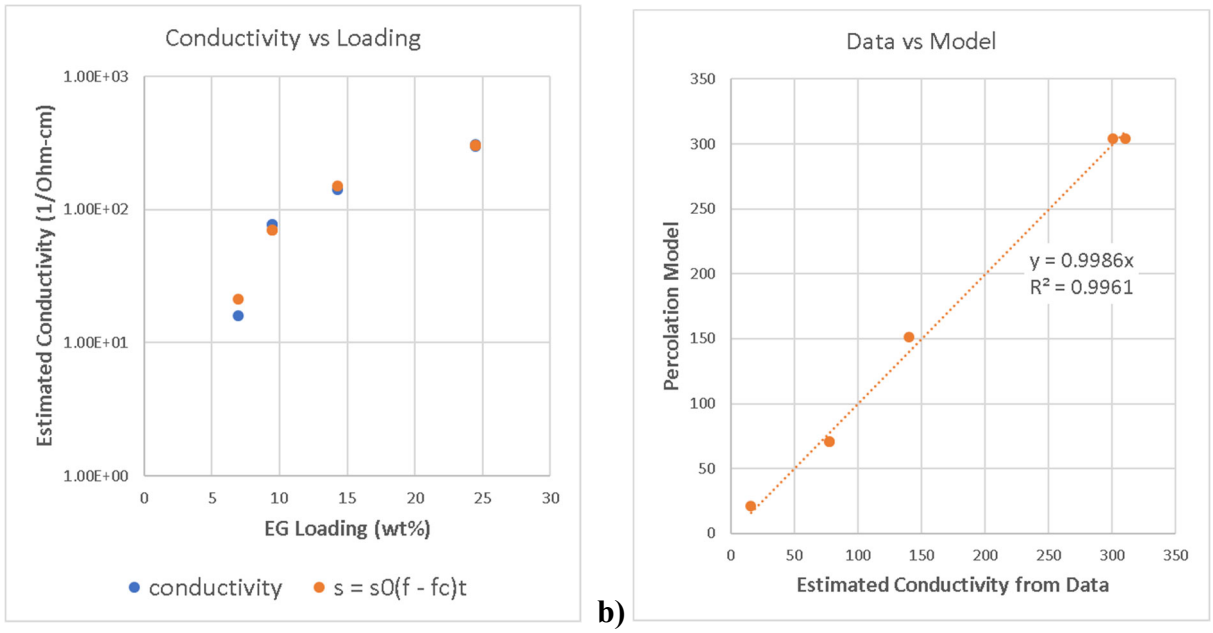
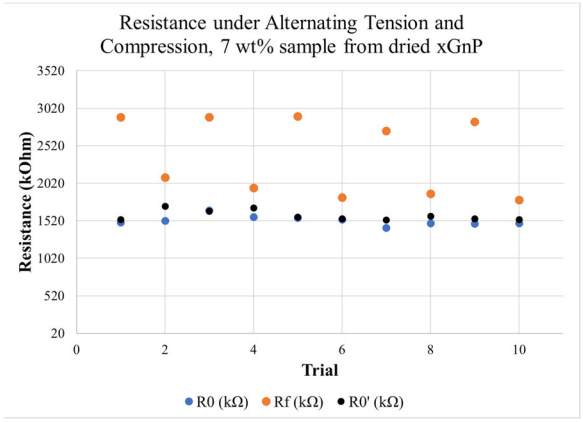
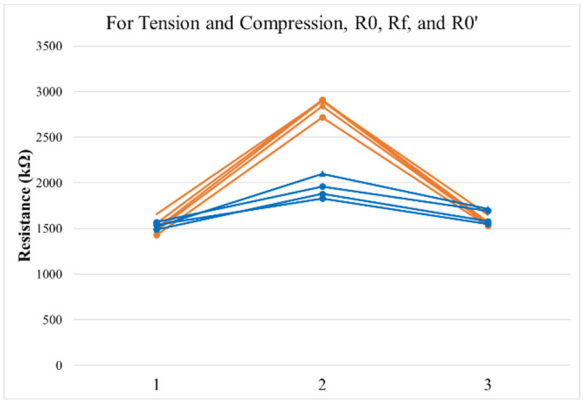


Figure 26. a) Conductivity estimated from the data (blue) and conductivity from the percolation model (orange) as a function of xGnP weight fraction in the dry film. b) Fit versus data.

16 GF of a High Resistance Sensor



a)



b)

Figure 27. a) Resistance during 10 strain trails, 5 each of tension and compression, of a 7 wt% xGnP sensor for which the xGnP dried completely after sonication and was remixed into EA before the addition of paint. Each trail recorded resistance in the initial unstrained state, R_0, resistance under either tension or compression, and resistance in the final unstrained state R_0'. b) The same data presented to show the tension (orange) and compression (blue) trials overlaid.

17 Testing Mechanical Integrity of Sensor vs. xGnP Loading

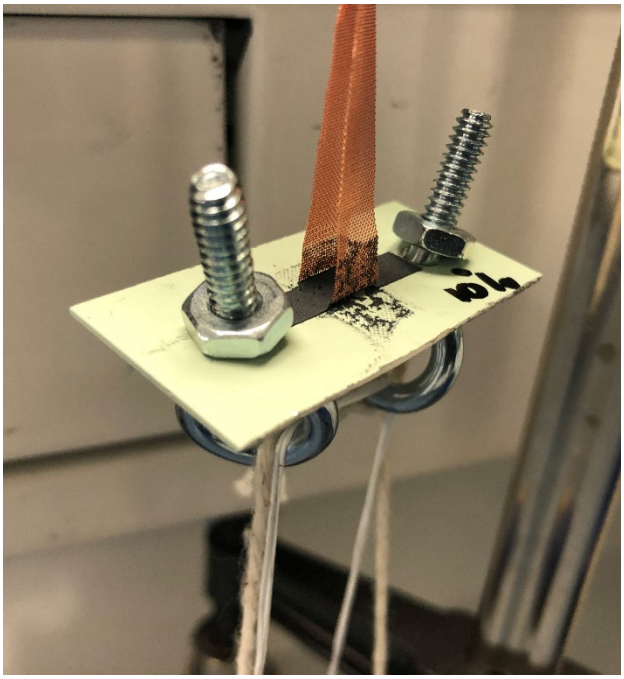
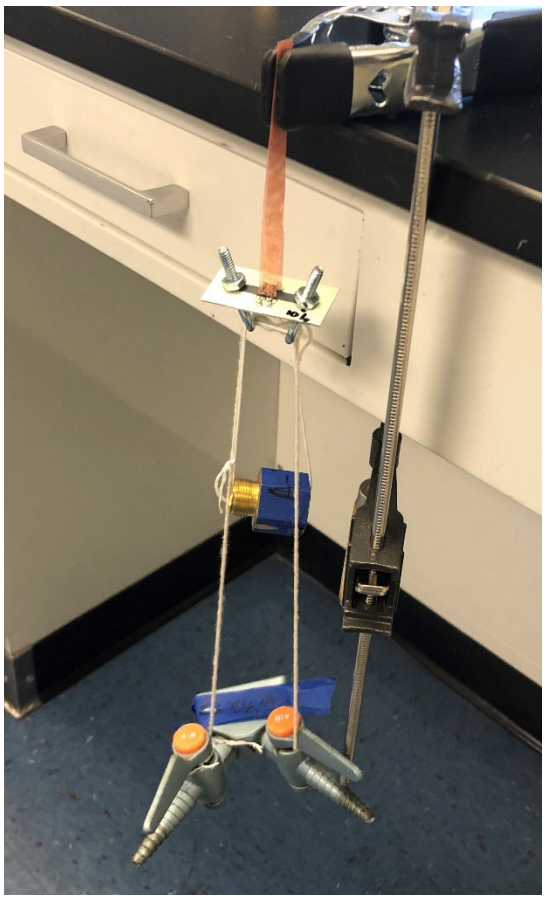
a)  b) 

Figure 28. Photographs showing the tests that generated the data in Figure 3. a) Close-up view of Cu mesh embedded in sensor painted on small coupon. b) Overview of clamp holding the Cu mesh, and objects of known weight loading the coupon.

18 Dynamic Strain Response

It is of interest in SHM to monitor vibrations of aircraft components. To obtain the dynamic response, the cantilever of Section 3.3 was deflected downward by 5 cm to place the cantilever in tension and released; the cantilever vibrated at its characteristic frequency (35.5 Hz obtained from a sine wave fit) with a decaying amplitude, as shown in Figure 29 for three trials. The strain gauge was able to follow this motion. We had previously shown that xGnP/latex strain gauges were able to follow at least 100 Hz, and these strain gauges are also fast. However, the positive gauge factor in compression distorted the shape of the curve: rather than going to a negative value, the resistance stayed positive at the larger deflections. Nevertheless, the xGnP paint sensors are able to track vibrations.

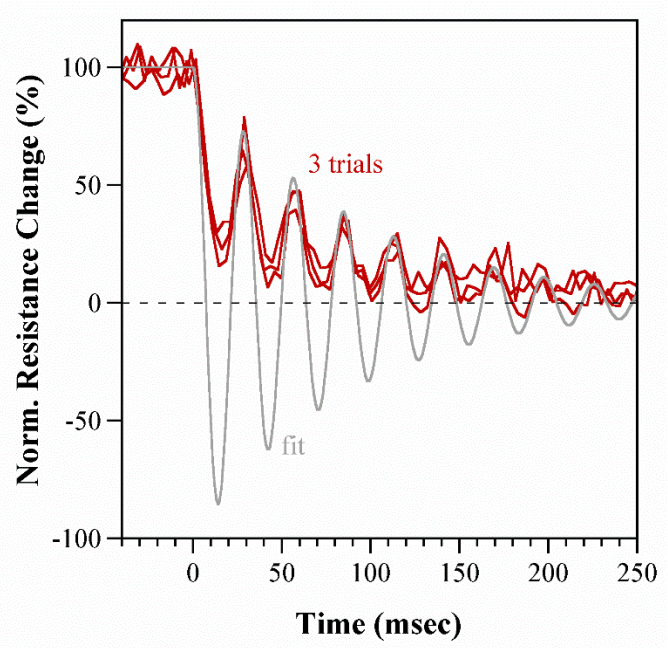


Figure 29. Normalized resistance change over time from the sensor of Figure 4b on a vibrating cantilever; three trials (red). A damped exponential curve fit (gray) is also shown (frequency f = 35.5 Hz, damping coefficient ζ = 0.05). (6.85 wt% xGnP, initial tip deflection 5 cm)

19 Additional Temperature and Humidity Data

The resistance and temperature versus time data used in Figure 5a are shown in Figure 30. The resistance of a sensor was monitored continuously using the microprocessor, while the temperature was measured periodically with the IR thermometer.

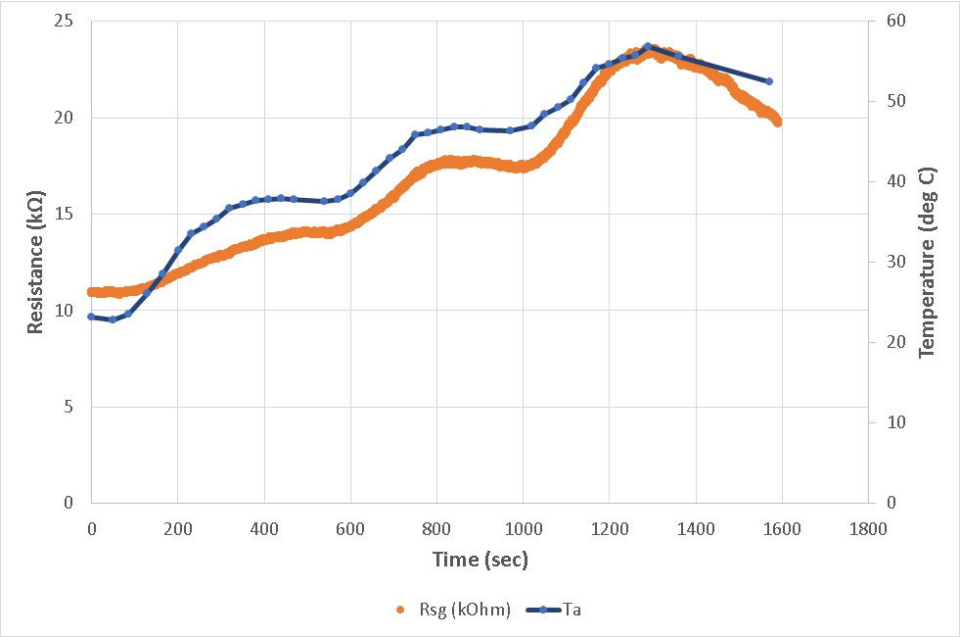


Figure 30. Resistance (orange) and temperature (blue) of a 7 wt% xGnP paint sensor over time as the temperature of a hotplate was raised to three levels over the course of 25 minutes.

Figure 31 shows the results as the temperature of the hot plate increased after being set to 100 °C, and also after the sensor was removed and set onto a room-temperature countertop (at time t = 355 sec). The dependence of resistance on temperature is confounded in such an experiment by the sample not reaching a steady state and by the driving off of moisture during the initial temperature increase.

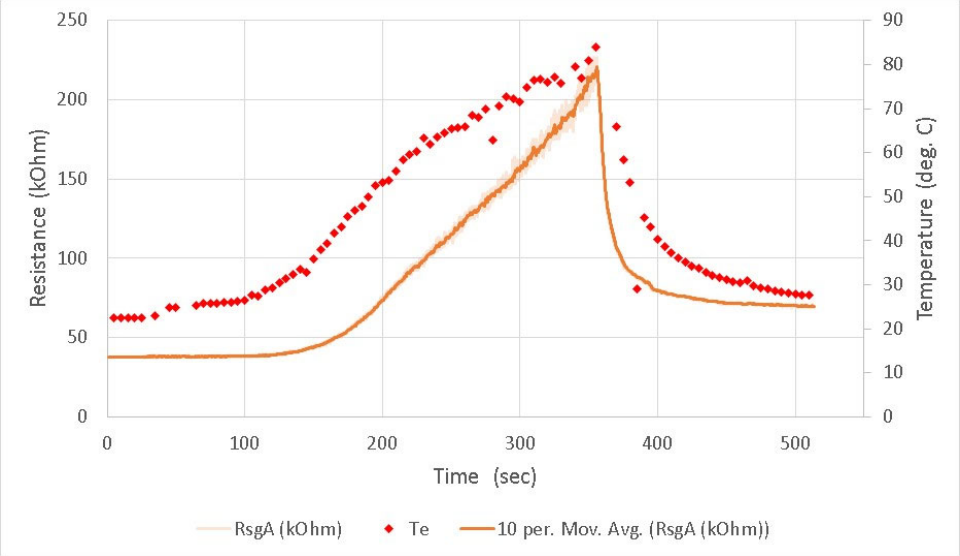


Figure 31. Resistance (orange) and temperature (red) of a 7 wt% xGnP paint sensor over time as the temperature of the hotplate increased steadily.

Figure 32a shows simultaneous readings from the data logger of temperature and humidity and resistance readings from the sensor by the microcontroller. Before $t = 0$, the data logger was placed inside a sealed chamber at 100% RH. At $t = 0$, the strain gauge was added to the chamber. At $t = 19$ hours, both the logger and the strip specimen were removed from the bin and placed at room temperature and humidity. Over the subsequent days, the humidity fluctuated with the weather, but the temperature remained constant. The resistance of the sensor closely followed the humidity. Plotting the same data as R vs. humidity (Figure 32b) after 35 hours (Figure 32indicated by the arrow in Figure 32a), the relationship was found to be linear.

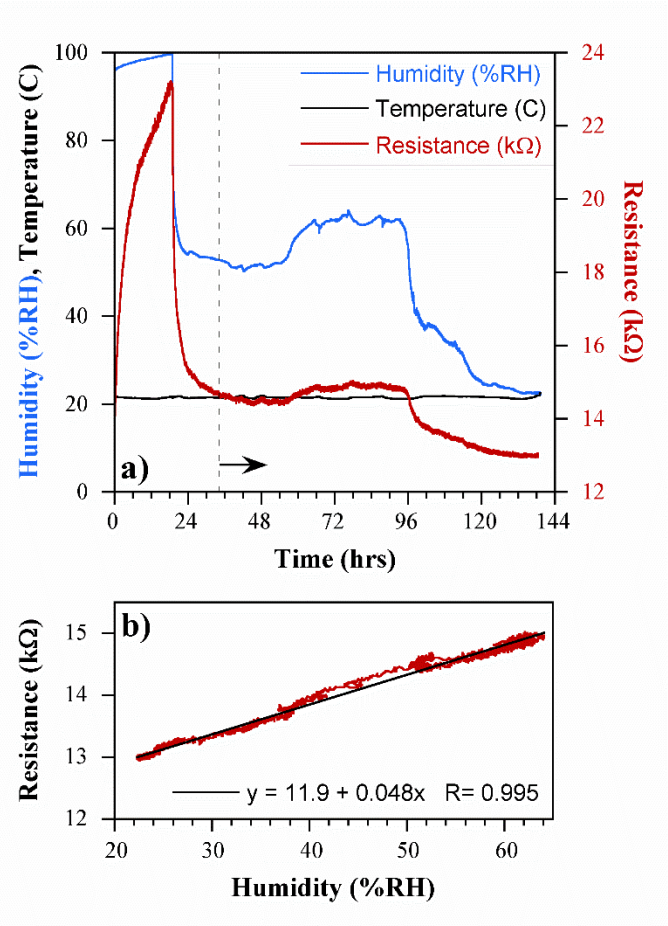


Figure 32. a) The relative humidity and temperature, and the resistance of a 7 wt% xGnP/paint sensor versus time. b) Resistance as a function of humidity.

20 Repair of xGnP-Latex Paint Sensor

A U-shaped sensor was formed on a latex primer-coated steel beam (Figure 33). The layers on the beam were: latex-based paint primer, xGnP-latex, and latex only; the final latex served as a mechanically protective layer. Additional information about these sensors can be found in [35]. The specimen had been damaged due to handling and numerous strain experiments. Damage at the base of the beam, near the Cu foil contacts, is shown in Figure 34.

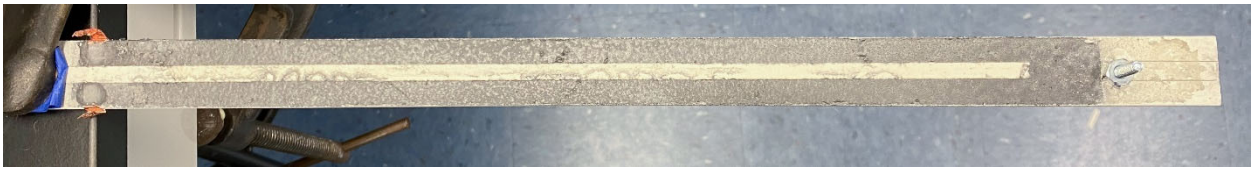


Figure 33. U-shaped xGnP-latex paint sensor on a primer-coated steel beam, covered with a protective layer of latex.

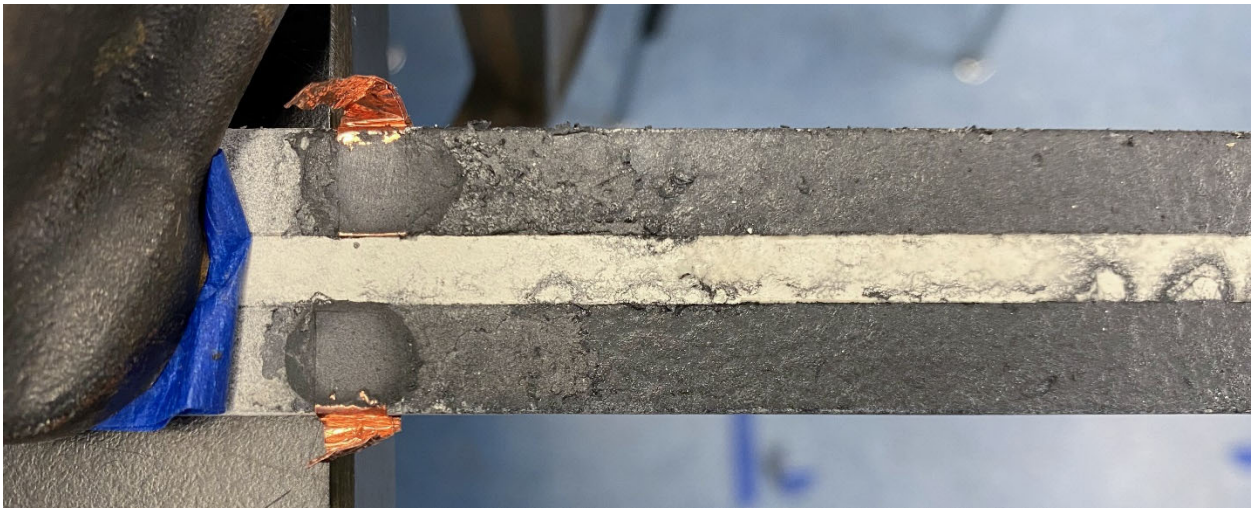


Figure 34. Close-up of damage near the Cu tape contact, on the top half of the U.

The three layers around the area of damage were removed using the abrasive side of a scrubbing sponge. The damaged surface was sanded in such way that each layer was exposed in a gradient, so that each could be accessed. For example, the top latex protective layer was removed to expose the xGnP-latex sensing layer, for later contact to it by the repair layer. The xGnP-latex was removed to expose the primer, to ensure that the primer added during repair was continuous with this layer and completely covered the steel.

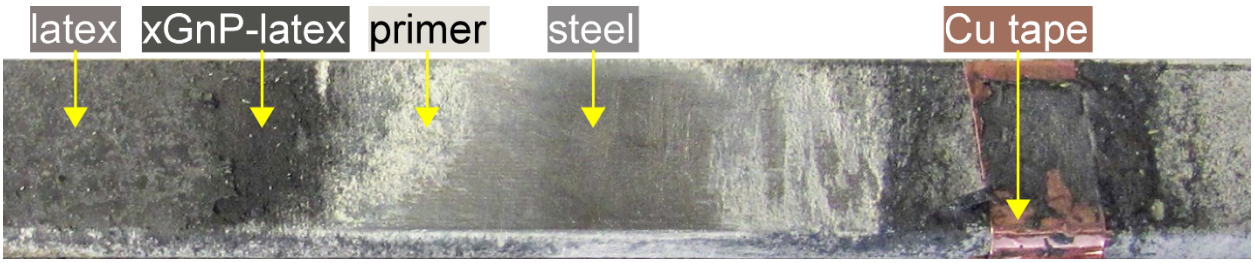


Figure 35. Close-up of damaged area after sanding down to the steel to expose all the layers. Note: the view is rotated 180° from the one in Figure 34.

The area to be coated with primer was masked, and the primer applied and allowed to dry. The area to be coated with fresh xGnP-latex was then masked, and new xGnP-latex spray-coated over the exposed xGnP-latex and exposed primer. Finally, a topcoat of sprayed latex was applied on top.

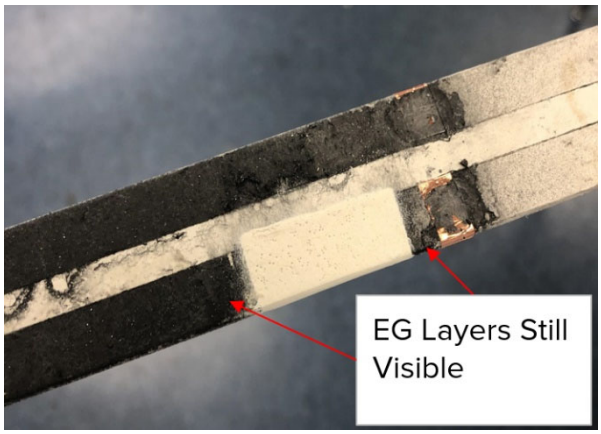


Figure 36. After adding primer up to the edges of the xGnP-latex.

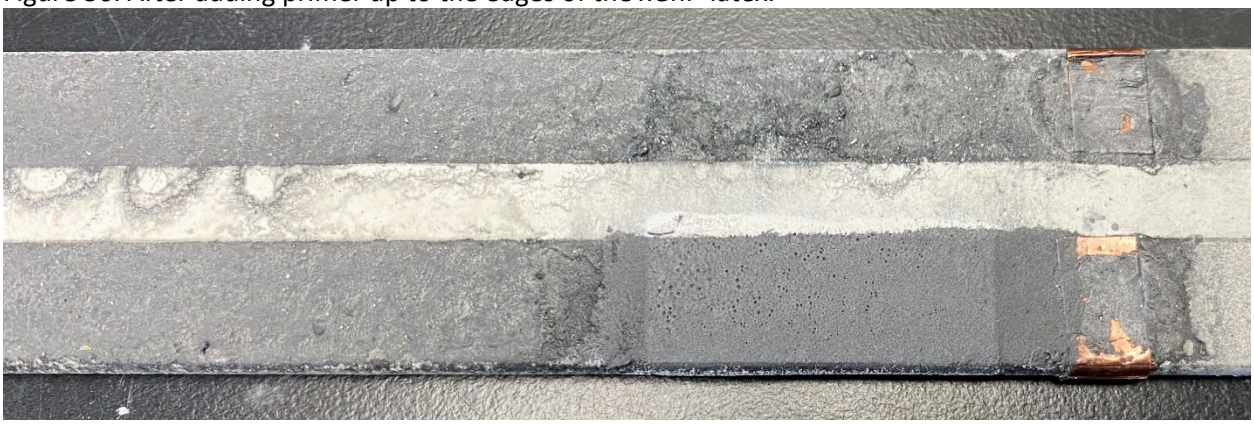


Figure 37. After adding xGnP-latex and a topcoat of latex.